Retinoid Content, Visual Responses, and Ocular Morphology Are Compromised in the Retinas of Mice Lacking the Retinol-Binding Protein Receptor, STRA6

Alberto Ruiz,[1] *Manuel Mark,*[2,3] *Hugues Jacobs,*[2,3] *Muriel Klopfenstein,*[2,3] *Jane Hu,*[4] *Marcia Lloyd,*[1] *Samer Habib,*[4] *Chinatsu Tosha,*[4] *Roxana A. Radu,*[4] *Norbert B. Ghyselinck,*[2,3,5] *Steven Nusinowitz,*[4,5] *and Dean Bok*[1,4,6]

Purpose. We report generation of a mouse model in which the *STRA6* gene has been disrupted functionally to facilitate the study of visual responses, changes in ocular morphology, and retinoid processing under STRA6 protein deficiency.

Methods. A null mouse line, *stra6 −/−*, was generated. Western Blot and immunocytochemistry were used to determine expression of STRA6 protein. Visual responses and morphological studies were performed on 6-week, 5-month and 10-month-old mice. The retinoid content of eye tissues was evaluated in dark-adapted mice by high performance liquid chromatography.

Results. STRA6 protein was not detectable in *stra6 −/−* null mice, which had a consistent reduction, but not total ablation of their visual responses. The mice also showed significant depletion of their retinoid content in retinal pigment epithelium (RPE) and neurosensory retina, including a 95% reduction in retinyl esters. At the morphological level, a reduction in thickness of the neurosensory retina due to shortening of the rod outer and inner segments was observed when compared to control litter mates with a commensurate reduction in rod *a*- and *b*-wave amplitudes. In addition, there was a reduction in cone photoreceptor cell number and cone *b*-wave amplitude. A typical hallmark in *stra6 −/−* null eyes was the presence of a persistent primary hypertrophic vitreous, an optically dense vascularized structure located in the vitreous humor between the posterior surface of the lens and neurosensory retina.

Conclusions. Our studies of *stra6 −/−* null mice established the importance of the STRA6 protein for the uptake, intracellular transport, and processing of retinol by the RPE. In its absence, rod photoreceptor outer and inner segment length was reduced, and cone cell numbers were reduced, as were scotopic and photopic responses. STRA6 also was required for dissolution of the primary vitreous. However, it was clear from these studies that STRA6 is not the only pathway for retinol uptake by the RPE. (*Invest Ophthalmol Vis Sci.* 2012;53:3027–3039) DOI:10.1167/iovs.11-8476

Vitamin A (all-*trans*-retinol) is an essential precursor for the generation of various functional derivatives, which include all-*trans*-retinaldehyde, all-*trans*-retinyl esters, and their stereoisomers. These retinoids participate in several important biological processes, such as reproduction, embryonic development, immune response, and vision.[1–3] Since mammals cannot synthesize retinol, diet is the main source of vitamin A, and it is stored initially in the liver as all-*trans*-retinyl esters until required for use in multiple tissues. Free retinol is unstable chemically and is highly insoluble in aqueous solution. The liver stores retinol as retinyl esters, which are enzymatically reversible. To transport retinol to other target tissues via blood circulation, a plasma retinol binding protein (RBP) and a thyroxine transthyretin (TTR) binding protein are needed to protect it from filtration by the kidney, oxidation, or enzymatic damage during the distribution process.[4,5] In the eye, retinol bound to RBP (holo-RBP) is delivered to the retinal pigment epithelium (RPE) through choriocapillaris blood. Since the mid-1970s, it was suggested that holo-RBP interacts with the basal side of RPE cells via a putative RBP receptor.[6–8] Accordingly, using RPE cells and a photo-cross linking reagent combined with high affinity purification, an RBP receptor protein was characterized and found localized on the basal side of these cells.[9] This receptor now is identified as STRA6, a polytopic membrane protein that binds to RBP with high affinity and mediates retinol uptake from the holo-RBP complex.[9] STRA6 has been proposed to possess a dual function as a membrane receptor and a membrane transporter.[9–11] While it is clear that STRA6 carries out the catalytic extraction of retinol from RBP, the precise pathway that retinol takes to reach its intracellular binding partners remains elusive.[12] STRA6 also is expressed in other tissues responsible for retinol processing, like skin, choroid plexus, placenta, and testis.[13–15] Human *STRA6* mutations are associated strongly with severe pathological phenotypes, particularly at the embryonic stage. The consequences of these mutations are

From the [1]Department of Neurobiology, [4]Jules Stein Eye Institute, and [6]Brain Research Institute, David Geffen School of Medicine, University of California at Los Angeles, Los Angeles, California; and the [2]Institut de Génétique et de Biologie Moléculaire et Cellulaire, [3]Université de Strasbourg, Illkirch, France.

[5]NBG and SN made equal contributions.

Supported by USPHS Grant EY00331 and grants from the Macula Vision Research Foundation. The STRA6$^{tm\ 1\ Nbg}$ mouse mutant line was established at the Institut Clinique de la Souris (ICS) (Mouse Clinical Institute [MCI]), Illkirch, France (http://www.ics-mci.fr/) in the Genetic Engineering and Model Validation Department with funds from NBG and MM, who were supported by Inserm, Fondation pour la Recherche Médicale Grant DEQ20071210544 (FRM) and Agence Nationale de la Recherche Grant 09-BLAN-0286-1 (ANR).

Submitted for publication August 25, 2011; revised February 15 and March 19, 2012; accepted March 22, 2012.

Disclosure: **A. Ruiz**, None; **M. Mark**, None; **H. Jacobs**, None; **M. Klopfenstein**, None; **J. Hu**, None; **M. Lloyd**, None; **S. Habib**, None; **C. Tosha**, None; **R.A. Radu**, None; **N.B. Ghyselinck**, None; **S. Nusinowitz**, None; **D. Bok**, None

Corresponding author: Dean Bok, JSEI 100 Stein Plaza Rm. B-182, Jules Stein Eye Institute, University of California, Los Angeles, CA, 90095; bok@jsei.ucla.edu.

manifested in a variety of disorders, which include pulmonary dysgenesis, cardiac malformations, mental retardation, and microphthalmia/anophthalmia, which are referred to collectively as Mathew-Wood syndrome.[16–18] Most recently, a variety of developmental abnormalities due to defects in retinol uptake and its processing also were reported in zebrafish with STRA6 partial deficiency.[19]

To examine the essential regulatory role of STRA6 on retinol uptake and processing by the RPE cells, we sought to generate a mouse model in which its expression was disrupted functionally.

The data presented in our report demonstrate that *stra6* −/− mice display an eye phenotype less severe than the pathological abnormalities observed in humans with mutations in the same gene. Our studies conclude that STRA6 is required for most of the retinol uptake process in the RPE, but also suggest the existence of alternative pathways that would compensate partially STRA6 function under compromised conditions.

Materials and Methods

Mice

Frozen embryos with a hybrid C57BL/6J (50%)-129Sv (50%) genetic background and heterozygous for the *stra6* mutation (*STRA6*$^{tm\ 1\ Nbg}$ allele, Fig. 1A; *stra6* +/−) were received from the Institut de Génétique et de Biologie Moléculaire et Cellulaire (IGBMC, Illkirch, France). Cryopreserved embryos went through a re-derivation process in surrogate females by the UCLA/Assisted Reproductive Technology (ART) core facility. Resulting offspring were genotyped by PCR of genomic DNA from tail biopsies. Genotyping was performed by using primers described in Supplementary Table S1 (http://www.iovs.org/lookup/suppl/doi:10.1167/iovs.11-8476/-/DCSupplemental), and the PCR core reagents (Applied Biosystems, Branchburg, NJ). Primers P1 and P2 were used for the detection of the wild-type gene (173 base pairs bp-long), and primers P1 and P3 for the detection of the *stra6* null allele (326 bp-long). Heterozygous mice (*stra6* +/−) were intercrossed to obtain the *stra6* −/− mutants used in our studies. All mice were maintained on a 12-hour light/dark cycle and fed ad libitum with NIH-31 modified open formula, which contains 24,500 IU/kg vitamin A acetate (Harlan Teklad, Madison, WI). All experimental procedures were performed on groups of mice at 6 weeks, 5 months, and 10 months of age. All experiments involving the use of mice were in compliance with guidelines established by the National Institutes of Health, and by the ARVO Statement for the Use of Animals in Ophthalmic and Vision Research.

Western Blot Analysis

Proteins from freshly dissected tissues were extracted as described previously.[20] Ten micrograms of sample were used for each analysis. Electrophoresis and immunodetection were carried out as described previously.[20] Primary antibodies included: rabbit anti-STRA6 peptide (from IGBMC), rabbit anti-RPE65 peptide (M.T. Redmond), rabbit anti-RGR peptide (H. Fong), rabbit anti-LRAT peptide (D. Bok), and a commercial monoclonal anti-GAPDH (sc-51905; Santa Cruz Biotechnology Inc., Santa Cruz, CA).

Retinoid Analysis

All mice were dark-adapted overnight, and all tissue manipulations were performed under dim red light (Eastman Kodak Co., Wratten 1A filter). Each retina and eyecup containing RPE were processed and analyzed by normal-phase high performance liquid chromatography (HPLC) as described previously.[21] Identification of each retinoid was confirmed by on-line spectral analysis and co-elution with authentic retinoid standards.

Fundus Imaging

Fundus images were obtained using the Micron II retinal imaging microscope (Phoenix Research Laboratories, Inc., Pleasanton, CA). Mice were anesthetized with an intraperitoneal (IP) injection of normal saline solution containing ketamine (15 mg/g) and xylazine (7 mg/g body weight), and pupils were dilated with a drop of 1% atropine sulfate. The mouse eye was aligned with the optical axis of the camera, with the objective lens positioned so that it touched the corneal surface (corneal applanation). Serial images were recorded to document the change in retinal and ocular appearance over the course of the study.

Retinal Angiography

Retinal angiography was performed using the same general fundus imaging procedure described above. Mice were anesthetized and injected IP with 10% sodium fluorescein (Akorn Inc., Decator, IL) at a dose of 0.01 mL per 5–6 gm body weight. Short-wavelength light (1_{max} = 487 nm) was used to excite the fluorescein, and a blocking filter (transmission <500 nm <0.1%) was placed in the optical pathway to prevent the excitation light from reaching the camera. A movie of approximately 10 minutes' duration was recorded from which individual images and clips were extracted.

Spectral Domain Optical Coherence Tomography (SD-OCT)

Ultra high resolution SD-OCT imaging was performed with a commercially available SD-OCT system designed specifically for the mouse (Bioptigen, Research Triangle Park, NC). A series of 100 *b*-scans were collected, stacked and aligned spatially to form a registered three-dimensional rendering of retinal volume (see Supplementary Fig. S1, http://www.iovs.org/lookup/suppl/doi:10.1167/iovs.11-8476/-/DCSupplemental). A high resolution *b*-scan from superior to inferior retina centered on the optic nerve head was captured by averaging and spatially aligning 20 individual *b*-scans along the same vertical axis. The resulting images were exported as 640 × 480 pixel 8 bit grey bitmap files, and processed in Adobe Photoshop CS3 (Adobe Systems, San Jose, CA).

Electroretinogram (ERG)

ERGs were recorded as described previously.[22] Briefly, after overnight dark-adaptation, ERGs were recorded from the corneal surface of the eye using a gold-loop electrode referenced to a similar gold wire inserted in the mouth. The mouse eye was positioned in front of an opening in a large integrating sphere in which brief flashes of light were presented. Responses to these light flashes were amplified 10,000× (Grass P511 High Performance AC Amplifier), band-pass filtered (0.1–300 Hz), digitized using an I/O board (PCI-6221; National Instruments, Austin, TX) in a personal computer, and averaged. Rod-mediated responses were recorded to blue flashes (Wratten 47A, λ_{max} = 470 nm) after dark adaptation. Cone-mediated responses were recorded to white flashes on a rod-saturating background (32 cd/m^2). All stimuli were presented at 1 Hz except for the brightest flashes, where the presentation rate was slowed to 0.2 Hz.

Histology

Paraffin Embedded Tissue. Heterozygous mice were mated, and 12 PM of the day of vaginal plug appearance was taken as 0.5 day post-coïtum (E0.5). Embryos and fetuses were collected by cesarian section at selected time points, and were fixed in Bouin's fluid for 5 days, embedded in paraffin, and serially sectioned at a thickness of 5 μm. Before paraffin embedding, E18.5 fetuses were treated for 30 hours in DC3 decalcifier (Labonord, Templemars, France). Sections then were stained with hematoxylin and eosin according to standard procedures.

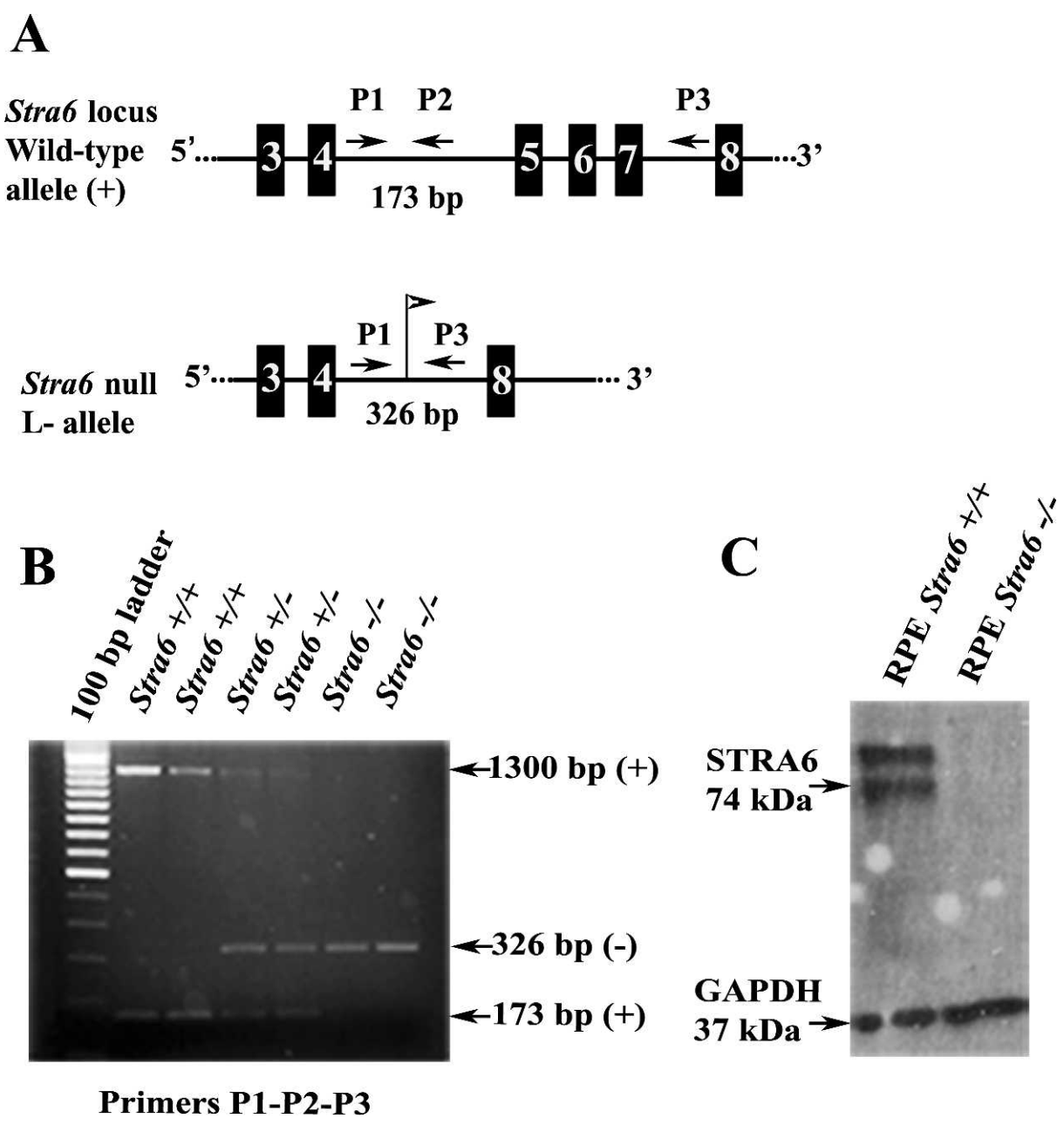

Figure 1. Genotyping of the wild-type and mutant alleles was done by PCR on genomic DNA samples from tail biopsies, and absence of STRA6 protein from RPE cells was confirmed subsequently by Western Blot analysis. (**A**) A genomic region that includes the area encompassing exons E3 through E8 (*numbered solid boxes*) of the *stra6* wild-type allele (*top*). In the *stra6* null (L−) allele, the fragment containing exons E5 to E7 was replaced by a single LoxP site (flag), making the *stra6* gene non-functional (*bottom*). Position and orientation of DNA primers (P) used for genotyping are indicated by arrows. (**B**) A representative image from PCR amplifications obtained by the combination of primers described in (**A**). (**C**) Western Blot image using RPE cell extracts from *stra6* −/− mutant and WT control. Immnunodetection was performed with a polyclonal antibody against a C-terminal peptide of mouse STRA6 and a monoclonal anti-GAPDH as internal control.

Plastic Embedded Tissue. Mice anesthetized with isoflurane were fixed by intracardiac perfusion. Light cautery was applied at the superior pole of the cornea to mark the orientation before enucleation of the eyeball. The eye cup was trimmed into temporal and nasal hemispheres. All tissues were immersed for 1 hour in 1% osmium tetroxide dissolved in 0.1 M sodium phosphate buffer (pH 7.4) followed by dehydration in a graded series of alcohols.

The temporal hemispheres were embedded in an Epon/Araldite mixture. Light microscope sections were cut at 1 μm, and stained with 1% toluidine blue and 1% sodium borate, then photographed with a Zeiss Axiophot microscope fitted with a Planapo 63X oil-immersion lens and a CoolSNAP digital camera.

Immunocytochemistry and Confocal Microscopy

Mice were euthanized with isoflurane. The eyes were fixed in 4% formaldehyde. After the eyecups were infiltrated successively with 10% and 30% sucrose in phosphate buffer, they were embedded in OCT (Sakura Fine Technical Co., Torrance, CA). Ten micrometer frozen sections were cut on a cryostat (Leica CM3050S). The cryosections were re-fixed in 4% formaldehyde for 10 minutes and quenched with 50 mM ammonium chloride (NH4Cl). Cryosections were incubated with a blocking solution followed by incubation with affinity purified antibodies against a C-terminal peptide of STRA6 (1:200, abCam Inc. # ab73490). The sections were exposed to secondary goat anti-rabbit

IgG antibodies, conjugated to Alexafluor 488 (Molecular Probes, Eugene, OR) for 1 hour. The cone sheaths were labeled with fluorescein-tagged peanut agglutinin (PNA, 20 ug/mL; Vector Laboratories, Burlingame, CA). The sections were examined under a confocal laser scanning microscope (Fluoview, Olympus, Japan).

Retina Flat-Mount Preparation

Mice were euthanized with isofluorane, and the eyes were enucleated. The retina was separated from the rest of the posterior segment and was fixed in 4% formaldehyde. The retina was stained with fluorescein-tagged PNA (20 μg/mL) for an hour, cover-slipped and examined under a confocal laser scanning microscope (Fluoview, Olympus, Japan) with a 40× objective.

Results

Gene Disruption in the *stra6* −/− Mice

After re-derivation of cryopreserved embryos, heterozygous *stra6* +/− mice obtained from the F1 progenies were intercrossed for generation of the *stra6* −/− mutant with total disruption of the gene. PCR screening of genomic DNA from tail biopsies was used to differentiate genotypically *stra6* null mice from wild type (WT) and heterozygous litter mates (Fig. 1B). *stra6* −/− mice developed with normal appearance, which was unexpected when compared to outcome of *stra6*-null mutation in humans. Synthesis of STRA6 protein was not detected by an anti-STRA6 antibody raised against the C-terminal sequence of the mouse polypeptide, as opposed to *stra6* +/+, which showed a product with a molecular mass of about 74 kDa and an additional one of higher molecular weight (Fig. 1C). The fact that no proteins smaller than 74 kDa were observed in the *stra6* −/− extracts, rules out the possibility of re-initiation of translation downstream from the deleted region of the *stra6* mRNA. To confirm that an equal amount of protein was loaded from each cell extract, a commercial monoclonal anti-GAPDH antibody was used as an internal reference (Fig. 1C).

STRA6 Localization and Morphological Changes in the Retina of Null Mice

A slight reduction in eye diameter was noticed in specimens from 6-week-old *stra6* −/− mice. These observations were recorded by measuring freshly dissected eyeballs from WT and *stra6* −/− mice using a calibrated scale under light microscopy. The reduction in size was 8–10% in eye diameter, which persisted in *stra6* −/− mice at 5 and 10 months of age, respectively (Fig. 2). Cellular localization of STRA6 protein on whole retinal samples was imaged by immunocytochemistry and confocal microscopy. Representative images presented in Figure 3 show no STRA6 signal in RPE cells or any other surrounding cells in tissue sections coming from 6-week-old *stra6* −/− mice (Fig. 3B). In contrast, a strong fluorescent signal was observed in control tissue sections on the basolateral side of RPE cells, which is consistent with the expected localization of the RBP receptor (Fig. 3A and inset). In addition, light microscopy of plastic sections revealed a shortening in the length of inner (IS) and outer (OS) segments of *stra6* −/− retinas, compared to control mice (Figs. 3C, D). Variations in IS/OS thickness along the entire extent of the retina were observed. To illustrate these differences, a morphometric analysis of each WT and mutant eye was performed for inferior and superior hemispheres (at equally spaced points, eight for each hemisphere). This analysis demonstrated a consistent reduction in inner/outer segment length in *stra6* −/− eyes (Fig. 3E).

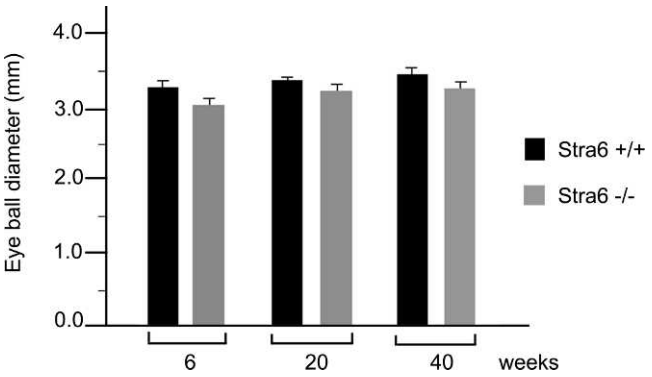

Figure 2. Comparison of eye diameter between *stra6* −/− and WT mice. Eyeballs were collected at 3 different ages, 6 weeks, 20 weeks (5 months), and 40 weeks (10 months). Measurements were recorded under stereo microscopy. Each value represents the average of 3–5 eyeballs from each WT and *stra6* −/− group of mice.

Effect of STRA6 Disruption on Other RPE Proteins

To determine if, due to the lack of STRA6, there was any variation in the expression of proteins present normally in RPE cells, we performed Western Blot analysis for visual cycle proteins RPE65, RGR, and LRAT. As seen in Supplementary Figure S2 (http://www.iovs.org/lookup/suppl/doi:10.1167/iovs.11-8476/-/DCSupplemental), protein extracts from RPE cells of *stra6* +/+, *stra6* +/−, and *stra6* −/− mice showed no difference in the levels of expression among the three genotypes. Conversely, STRA6 expression was higher in control *stra6* +/+ than heterozygous *stra6* +/− and was undetectable in the *stra6* −/−. From these results we conclude that STRA6 expression was disrupted effectively in RPE cells, and its absence had no repercussion on expression levels of other visual cycle proteins whose reduced expression would cause attenuation of the visual cycle.

Persistent Hyperplastic Primary Vitreous (PHPV) in the Eyes of *stra6* −/− Mice

SD-OCT and fundus imaging studies were performed routinely on all *stra6* mice before further evaluation. After analyzing several eyes from 6-week-old *stra6* −/− mice, dense "asteroid-like" bodies were apparent by fundus examination. These structures were localized in the vitreous humor and posterior to the lens. An IP injection of fluorescein allowed us to view their vascularization (Figs. 4A, B). A movie of blood flow through this structure is provided in the Supplementary Material (http://www.iovs.org/lookup/suppl/doi:10.1167/iovs.11-8476/-/DCSupplemental). A representative fundus image of the "asteroid-like" structure is displayed in Figure 4C. These structures contained many pigmented cells resembling choroidal melanocytes (Fig. 4D). Further analysis identified them as persistent PHPV. The primary vitreous body is a transient embryonic structure consisting of fibroblastic cells stemming from the periocular mesenchyme and a capillary network given off by the hyaloid artery.[23] Between E13.5 and E14.5, the fibroblasts forming the primary vitreous body (PV, Fig. 5A) become dispersed within the rapidly expanding, acellular, secondary vitreous body (SV, Fig. 5A), and are no longer identified at E15.5 (not shown). At E13.5, *stra6* −/− and WT eyes were indistinguishable histologically ($n = 3$). However, at E14.5 the number of cell nuclei in the secondary vitreous was markedly increased in *stra6* −/− fetuses compared to the WT ($n = 3$ for each genotype; compare PV, Figs. 5A, B, and data not shown). Later, E18.5 *stra6* −/− mutants ($n = 3$) showed a

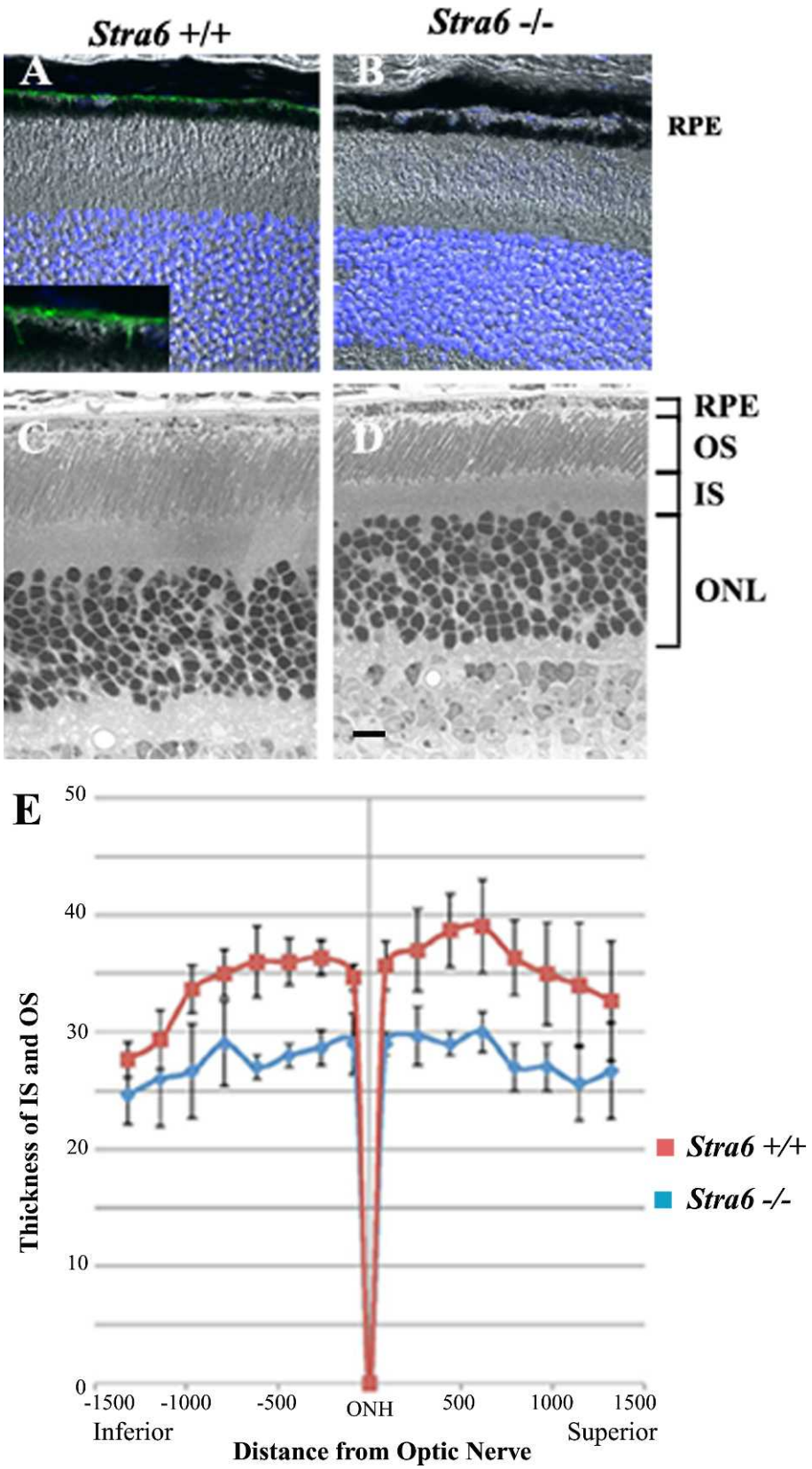

Figure 3. Histological features of the retina in *stra6* mutants and controls. (**A**, **B**) Frozen sections (10 μm) of retina from *stra6* +/+ and *stra6* −/− mice. STRA6 staining was performed by using the anti-STRA6 antibody from abCam Inc. at 1:200 dilution. (**C**, **D**) Images of 1 μm plastic sections of retina from both genotypes showing the shortening of outer segments and inner segments in the retina of mice lacking STRA6 (**D**). (**E**) Measurements of outer/inner segment thickness along the entire extent of the retina. The optic nerve head (ONH) was used as a point of reference to differentiate the superior (*right*) and inferior (*left*) hemispheres. Means of four representative retinas are shown for each *stra6* +/+ and *stra6* −/− genotype. Eight different points were measured in each hemisphere. ONL, outer nuclear layer. Bar, 20 μm.

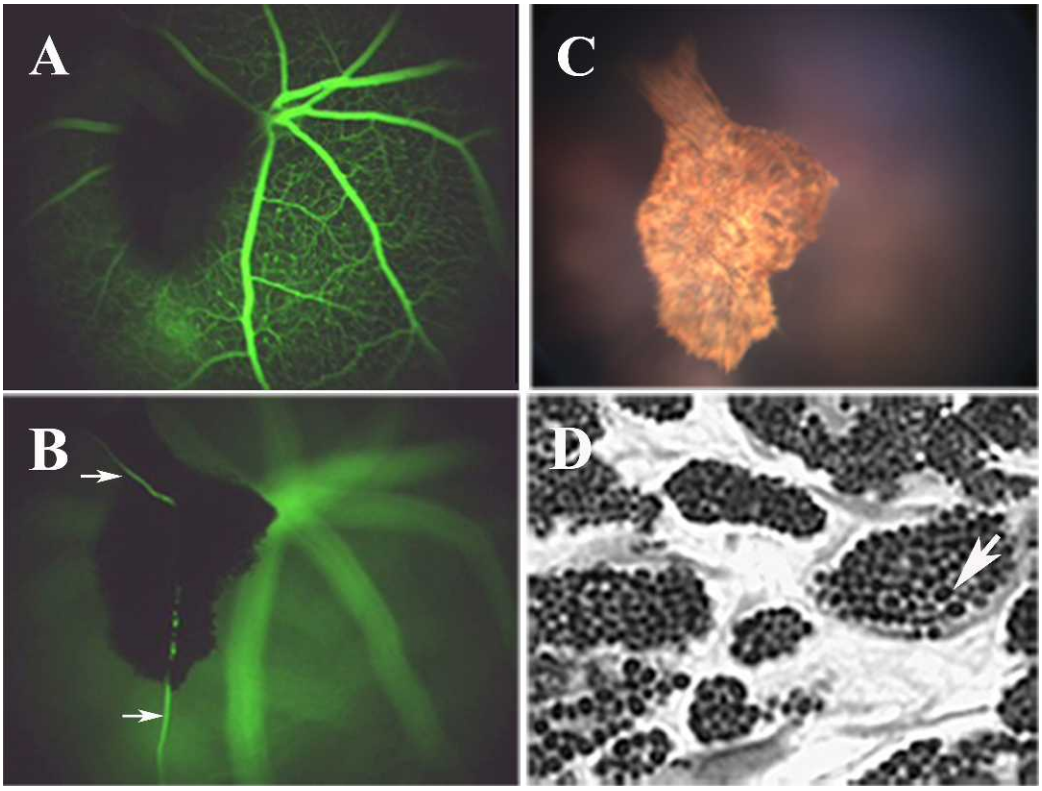

Figure 4. Representative fundus analysis and light microscopy images from a 6-week-old *stra6* −/− mouse are shown. (**A**, **B**) The presence of a PHPV structure in two different focal planes observed following IP injection of fluorescein. Vascularization of these structures is observed by the presence of blood vessels (**B**, *arrows*). (**C**) The asteroid-like appearance of the PHPV structure from (**A**) and (**B**) in standard fundus imaging. (**D**) Epon-Araldite sagittal section (1 μm) showing the internal features of the PHPV body, which includes pigmented melanocytes.

small mass of densely packed cells in the secondary vitreous body (PHPV, Fig. 5D) that was never observed in the WT ($n = 3$, Fig. 5C). All 2-month-old, adult, *stra6* −/− mutants ($n = 11$) exhibited a conical mass of cells between the optic nerve exit point and the lens (PHPV, Figs. 5F, H), whereas no PHPV was ever observed in the eyes of their WT litter mates ($n = 6$, Figs. 5E, G). PHPV also were observed in adult, *stra6* −/− mice, namely at 5 and 10 months old (Fig. 6, and not shown). SD-OCT analysis of eyes of *stra6* −/− mice also revealed that, in some cases, the density of these PHPV structures was sufficient to block the path of infrared light penetration for OCT signal acquisition in the right (OD) and left (OS) eyes, as shown in Figure 7 (see arrows in bottom panels of the left group). SD-OCT images of eyes from 5-month-old mice shown in Figure 7 (bottom panels of the right group) were similar to retinas of 6-week-old null mice.

Additionally, the retinal thickness of 5-month-old *stra6* −/− mice was equivalent to the 6-week-old mice (Fig. 6, lower panels). An interesting morphological observation in *stra6* mutants was the finding of a 20% reduction in the number of cones stained with fluorescein tagged PNA in 6-week-old mice as opposed to an 80% reduction at 5 months of age in comparison to corresponding controls (Fig. 8).

Effect of STRA6 Deficiency on Visual Responses

Dark-adapted ERG recordings are shown in Figure 9 for *stra6* +/+, *stra6* +/−, and *stra6* −/− mice. This figure shows the average (+ 1 SE) ERG response amplitudes to progressively higher light intensities for each mouse genotype. For the *a*- and *b*-waves, response amplitudes for the *stra6* +/− mice were indistinguishable from those obtained from the *stra6* +/+ control mice. In contrast, ERG responses from *stra6* −/− mice were significantly smaller than those of the *stra6* +/+ control mice. On average, scotopic *a*- and *b*-wave amplitudes, reflecting performance of photoreceptors and middle retinal cells, respectively, were approximately 20% and 50% those of *stra6* +/+ control mice. Interestingly, in the case of 6-week-old null mice with unilateral presence of PHPV, recording in both eyes showed a similar reduction in amplitude as shown in Supplementary Figure S3 (http://www.iovs.org/lookup/suppl/doi:10.1167/iovs.11-8476/-/DCSupplemental), indicating that these structures had little effect on retinal function. Our morphological observations regarding reduced cone density in null mutants was supported by a reduced cone response to light stimulation in *stra6* −/− mice. Cone *b*-wave amplitudes were, on average, only 20% of the WT or heterozygous responses at 6 weeks of age. This did not change substantially with age (data not shown).

Effect of STRA6 Deficiency on Retinoid Content in Retinal Tissues

For the evaluation of retinoid content, mice corresponding to all three *stra6* genotypes were dark adapted overnight before the eyes were freshly dissected. RPE cells and neurosensory retina samples were collected as separate groups. As shown in Figure 10, the amount of all-*trans*-retinol (all-*trans*-ROL) found in RPE and retina samples from null mice was reduced consistently compared to heterozygous and WT samples (Figs. 10A, D). The same reduced pattern also was observed when mutant eyes were tested for other retinol derivatives, such as all-*trans*-retinyl palmitate (all-*trans*-RP) and 11-*cis*-retinyl palmitate (11-*cis*-RP) for RPE (Figs. 10B, C), and 11-*cis*-retinalde-

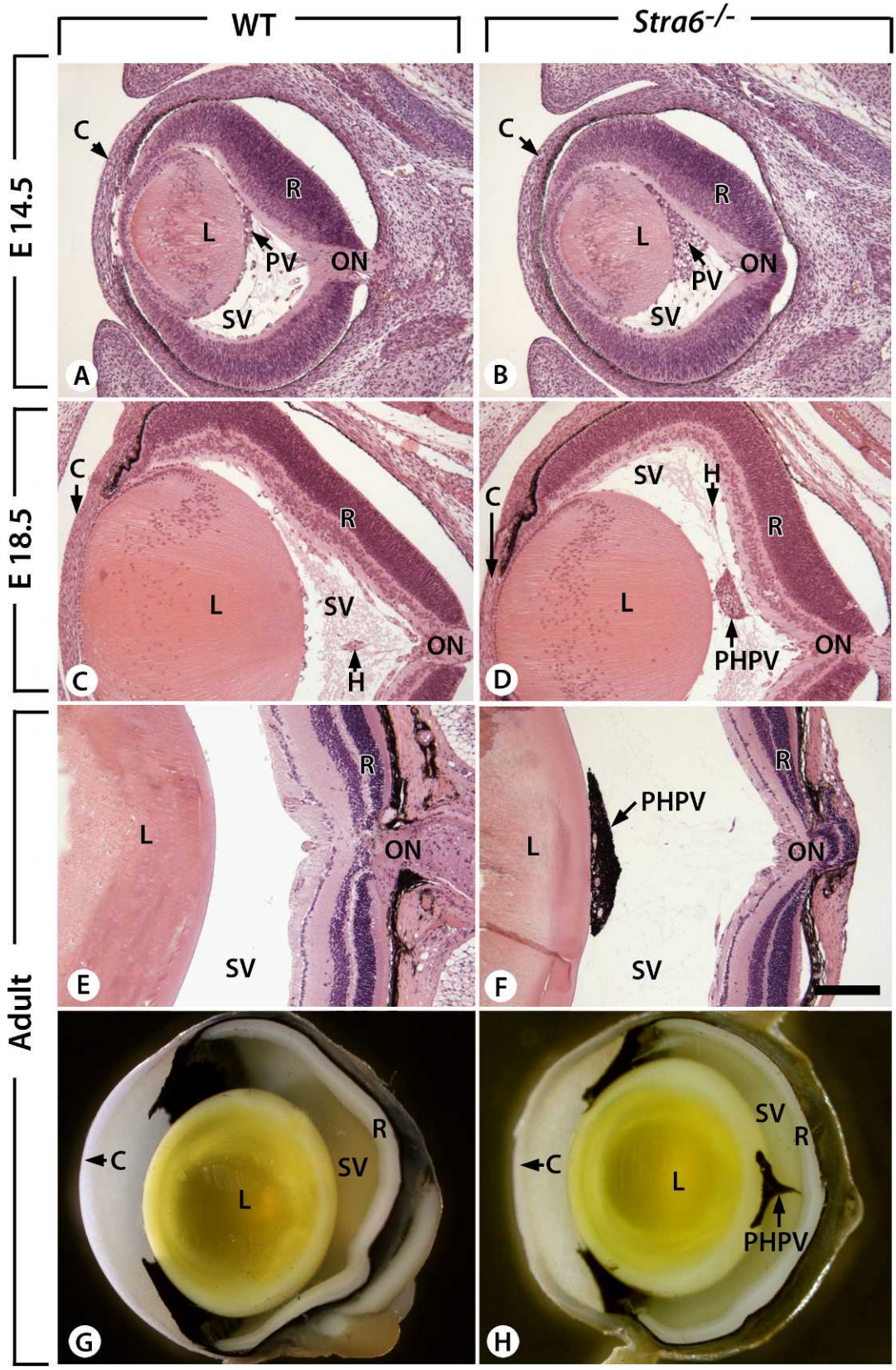

Figure 5. Ontogenesis of the persistent hyperplastic primary vitreous body in *stra6* −/− mutants. (**A–D**) Comparison of sagittal histological sections from E14.5 and E18.5 WT fetuses, and *stra6* −/− mutants (*stra6* −/−). (**E–H**) Comparison of 6-week-old WT and *stra6* −/− eyes. C, cornea; H, hyaloid vessel; L, lens; ON, optic nerve; R, retina. Bar indicates 160 μm (**A–F**).

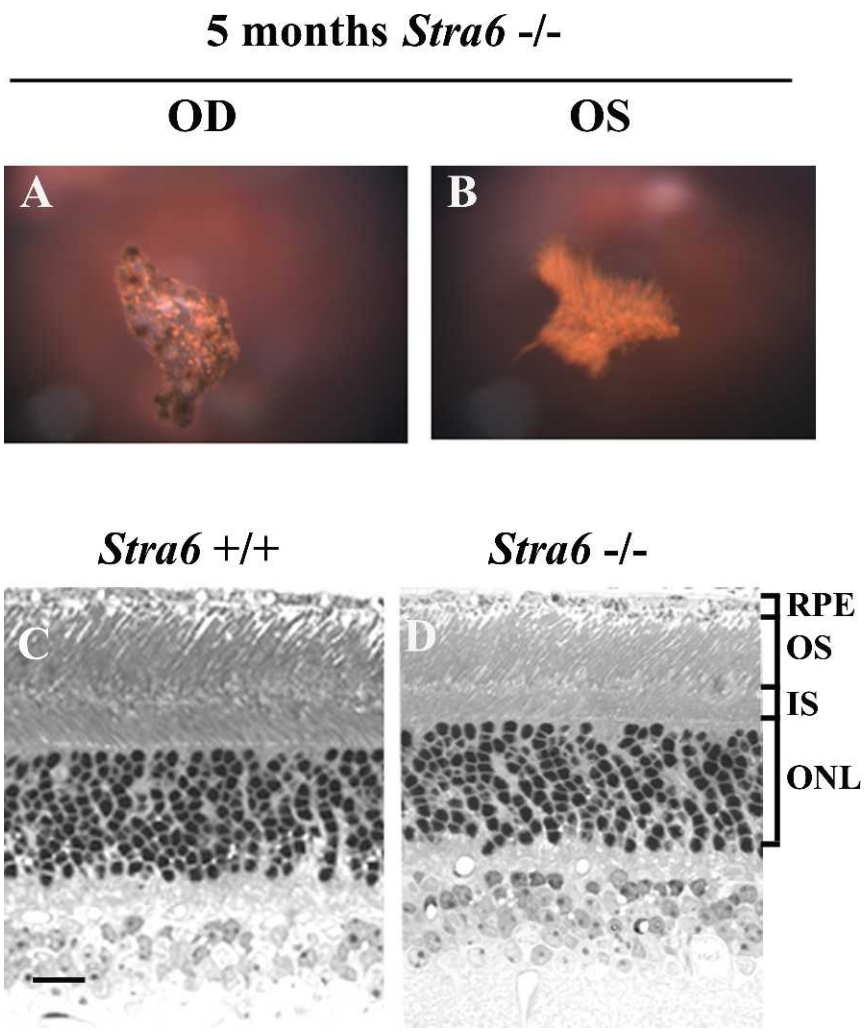

Figure 6. Fundus and light microscopy images from 5-month-old *stra6* mice. (**A**, **B**) Fundus images of a *stra6* −/− mouse showing the presence of PHVP in both eyes. (**C**, **D**) Light microscopy images revealing a reduction in the retinal IS and OS length for *stra6* −/− mice compared to WT controls. Bar, 20 μm.

hyde (11-*cis*-RAL) and all-*trans*-retinaldehyde (all-*trans*-RAL) for the retina (Figs. 10E, F), respectively. As shown in these panels, for overnight dark adapted mice, the vitamin A storage form (all-*trans*-RP) in the RPE cells showed the most dramatic variation with about 95% reduction in the *stra6* −/− extracts when compared to control samples (Fig. 10B). Interestingly, the *stra6* −/− mice were able to regenerate about 21% of the wild-type 11-*cis*-RAL levels (Fig. 10E) during dark adaptation, consistent with the photoreceptor response as indexed by the amplitude of the *a*-wave of the ERG (Fig. 9).

Discussion

Retinol is an essential component of the biological machinery needed by a living organism to achieve proper functioning throughout life. Due to the relevance of STRA6 as a membrane receptor for the retinol/RBP complex and its critical role as a retinol transporter,[9–11] we sought to generate a *stra6* null mouse model to provide a better understanding of the consequences of STRA6 deficiency in mammals. Severe phenotypic abnormalities have been associated with *stra6* mutations in human patients with Matthew-Wood syndrome.[16–18] Interestingly, the *stra6* null mice presented in our report show phenotypic variations that differ markedly from control litter mates, but are less severe than the ones observed in humans bearing *stra6* mutations.

An important phenotype in *stra6* −/− mutant mice was a reduction in retinal thickness due to shortening of their rod photoreceptor outer and inner segment lengths. Similar morphological changes were observed when other RPE proteins important for the processing of retinol derivatives were disrupted genetically in these cells, as in the case of RPE65[24] and LRAT.[25] However, it is important to mention that in the *rpe65* and *lrat* knock-out models the visual response as measured by ERG was virtually non-detectable as opposed to the *stra6* −/− mutant, where a significant, albeit abnormal, visual response to light stimulation remained. This significant ERG response suggests clearly that, despite the absence of STRA6 in the RPE, retinol or retinyl esters still were delivered and processed through the visual cycle for the generation of 11-*cis*-RAL. Therefore, the physiological effect of STRA6 ablation does not have the same impact as the disruption of partner proteins, like RPE65 and LRAT. This probably is due to the fact that, unlike RPE65 and LRAT, STRA6 is not directly responsible for the generation of 11-*cis*-retinoids.

The amount of retinol and its derivatives in RPE and neurosensory retina samples was much lower in *stra6* null

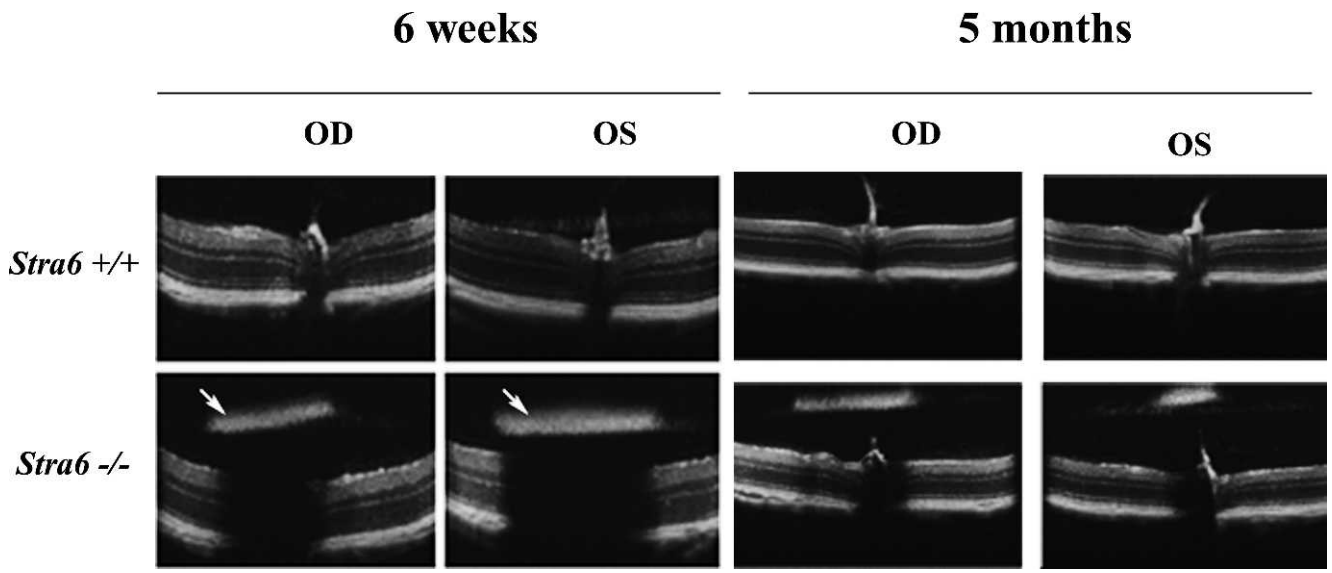

Figure 7. Representative SD-OCT showing the retinal features of *stra6* +/+ and *stra6* −/− mice at 6 weeks and 5 months. Images from 5-month group were taken at a lower magnification. Lower panel of 6-week-old mice shows the presence of asteroid-like dense structures (PHVP) above the retinal layers of both right (OD) and left (OS) eyes of *stra6* −/− mice (*arrows*). These structures were able to block the light path through the retina generating a shadow effect. However, in the lower panels of 5-month-old mice, despite the presence of PHVP in both eyes, the light path was not blocked, probably due to variability in the anatomical localization and degree of pigmentation.

mice. In both tissues, all-*trans*-ROL was considerably reduced to about 84% in the RPE and about 88% in the neurosensory retina, suggesting that the majority of retinol intake by RPE cells is STRA6 dependent. For RPE cells, all-*trans*-RP was depleted to a greater extent than any other retinoid (3% of control). Moreover, 11-*cis*-retinal was only 24% of controls in the neurosensory retina. This was in spite of the fact that in these mutants, LRAT and RPE65 showed no variation in their protein expression (suggesting full enzymatic activity). Nonetheless, even in the presence of reduced retinol uptake by the RPE, the amount of all-*trans*-RP available was sufficient to allow generation of enough 11-*cis*-RAL to provide a significant visual response. Interestingly, unlike *rpe65* and *lrat* null mice, there was no significant rod photoreceptor cell degeneration by 5 or 10 months, although the number of cone photoreceptors at that age was reduced considerably in *stra6* mutants. These findings resembled observations reported for *rpe65* and *irbp* knock-out mice,[26,27] and implied that retinoid levels are more

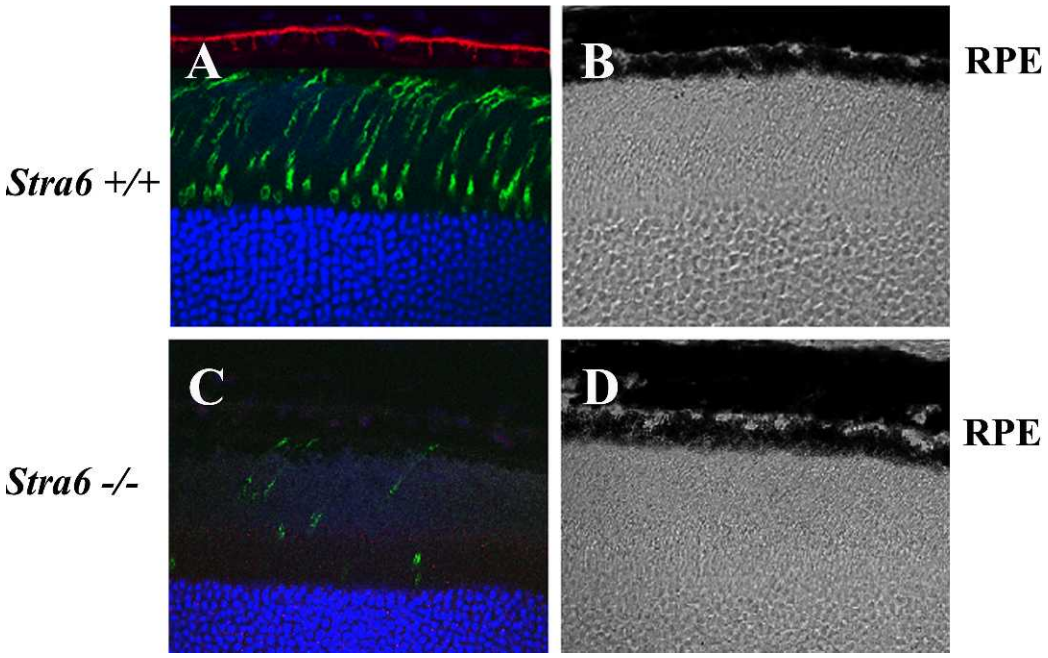

Figure 8. Histological features of the retina in *stra6* mutants and controls. Frozen sections (10 μm) of retina from 5-month-old *stra6* +/+ and *stra6* −/− mice are shown in all panels. Cone sheath staining (**A**, **C**) was obtained by using a fluorescein-tagged PNA (20 μg/mL). STRA6 staining (**A**) was performed by using the anti-STRA6 antibody from abCam Inc. at 1:200 dilution. (**B**, **D**) are Nomarski images of controls for *stra6* +/+ and *stra6* −/−, respectively.

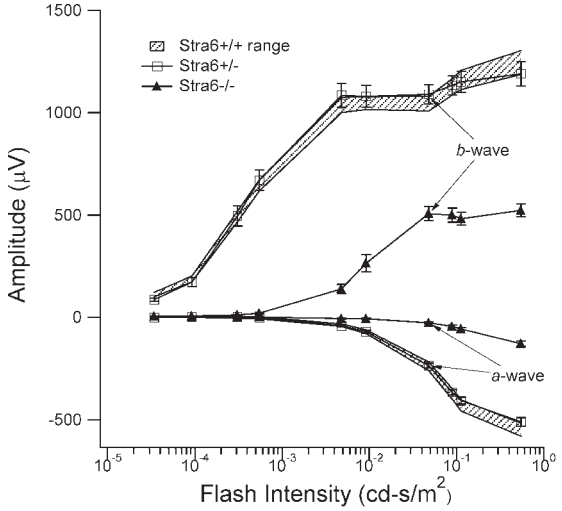

Figure 9. ERG analysis of 6-week-old *stra6* mice. ERG responses to blue-flash stimuli recorded under dark adapted conditions are shown for each group of mice. The shadowed regions define the normal ranges for *a*- and *b*-wave amplitudes for WT *stra6* +/+ mice. The responses from heterozygous *stra6* +/− mice fell completely within this range, consistent with normal retinal function. In contrast, ERG responses from *stra6* −/− mice were significantly smaller, with *a*- and *b*-wave amplitudes approximately 20% and 50%, respectively, of WT control and heterozygous mice. ERG analysis of 5-month-old *stra6* mice showed similar visual responses as the 6-week-old mice (data not shown).

critical for cone survival than for rods. Cones on the other hand, while present in higher numbers at 6 weeks of age, reduced their numbers to 20% of normal by 10 months. The effect on the cone *b*- wave amplitude was more dramatic. Even though cone numbers were higher at 6 weeks of age (70% of WT), their *b*- waves held steady at ~20% of normal between 6 weeks and 5 months.

Fundus imaging revealed the presence of dense bodies in the vitreous chamber of the *stra6* −/− mutant eyes, which resembled PHPV. Interestingly, PHPV represents the most frequent congenital abnormality of the rodent fetal vitamin A deficiency syndrome,[28,29] and it also is a characteristic feature of RARbeta and Raldh3 knock-out mice.[30,31] It was proposed previously that retinoic acid (RA) synthesized by Raldh3, which is expressed in the ventral retina and RPE,[31] activates RARbeta, which is expressed in the fibroblasts of the PHPV,[30] to control its normal involution during prenatal development. Our study shows that STRA6 also is instrumental to the involution of the PHPV. Involvement of STRA6 in this event most likely stems from its role in supplying RPE and retinal cells with vitamin A. Actually, as all-*trans*-ROL intake is considerably reduced in those cells, it is plausible that the amount of RA that can be synthesized by Raldh3 in the absence of STRA6 is not sufficient to allow proper activation of RARbeta in the primary vitreous body fibroblasts, and thereby arrest their proliferation. It is worth noting that although RA is required to prevent proliferation, impaired RA signaling does not interfere with cell differentiation, since the cells of the PHPV give rise to melanocytes, one of the differentiated cell-types normally arising from the periocular mesenchyme from which they originate.[30]

On retinal angiography, these PHPV structures were fed by blood vessels from the retina and choroid. Since in some cases the PHPV structures had sufficient density to block the light path during SD-OCT imaging, we wondered if the reduction of the ERG response in null *stra6* mice also was due partly to the obstruction of light reaching the retina rather than a physiological effect due to outer segment shortening. However, whether or not PHPV was present at 6 weeks or 5 months of age, the ERG responses observed in mutant mice always were reduced when compared to controls, and showed similar scotopic *b*-wave amplitude patterns for both eyes whether the presence of the PHPV structure was unilateral or bilateral. Therefore, the lower ERG response in mutants was due to the retinal changes caused by the lack of STRA6 and a direct consequence of reduced retinol intake, but not related to the dense structures themselves.

Our findings suggest clearly that STRA6 deficiency in these mutants had a significant impact at the physiological and biochemical level. However, they also demonstrate that its absence from the RPE does not abolish the visual response to light completely. These observations have interesting implications, because it is known that variability in loss of function exists for some of the human *stra6* mutations, and this is manifested by variable severity of the phenotype. It also has been reported that, when some of these mutations have resulted in full gene inactivation, the consequences were very dramatic, as in the total absence of eyes.[16–18] That was not the case for this model where, despite full disruption of the *stra6* gene, these mice showed a phenotype similar to that reported for young *rbp4*-deficient mice, which under normal diet (vitamin A sufficient), had impaired visual responses but otherwise were phenotypically normal.[32–34]

One must ask why such a phenotypic variation exists between humans and mice in the presence of abnormal STRA6 function. The most parsimonious explanation would be to refer to species-specific background gene differences. There are precedents for this from other studies. Examples include the generic *p53* knock-out[35] and the eye-related *abca4* (*abcr*) knock-out,[36–38] in which the phenotype in mice is not as severe as it is in humans with disruption of the same genes. These comparisons have taught us that there not always is a phenotypic correlation when orthologous genes are mutated in mice and humans, particularly when comparisons are drawn between genes that are disrupted in mice versus genes that carry point mutations in humans. In addition, environmental influence and differences in retinoid metabolism are likely different between humans and mice.

The other important question is, how do the null mice compensate for the lack of STRA6 function and cellular retinol intake? Our findings suggest clearly that STRA6 is not the only pathway for retinol uptake from circulating holo-RBP. This was evident from our earlier studies in which we disrupted the *lrat* gene conditionally and observed small amounts of retinyl esters in the RPE.[25] Therefore, alternative mechanisms for retinol intake must exist. Before the identification of STRA6 as an important membrane protein responsible for retinol uptake, several hypotheses were proposed in the literature for that role. These mechanisms included passive diffusion of free-retinol through cellular membranes,[14,39] retinoid delivered via the systemic circulation as chylomicrons,[40] and a putative role involving megalin as an endocytic holo-RBP receptor (Han et al., unpublished data).[41,42] It is possible that one or a combination of them could be playing a role in this process after all.

In summary, our studies provide a useful mouse model for the study of STRA6 function in ocular intracellular retinol transport. These mice will be important particularly for studies involving vitamin A deprivation. Along these lines, the use of combinatorial gene knock-out with this model also would advance our understanding further of the mechanisms underlying retinoid trafficking in the RPE.

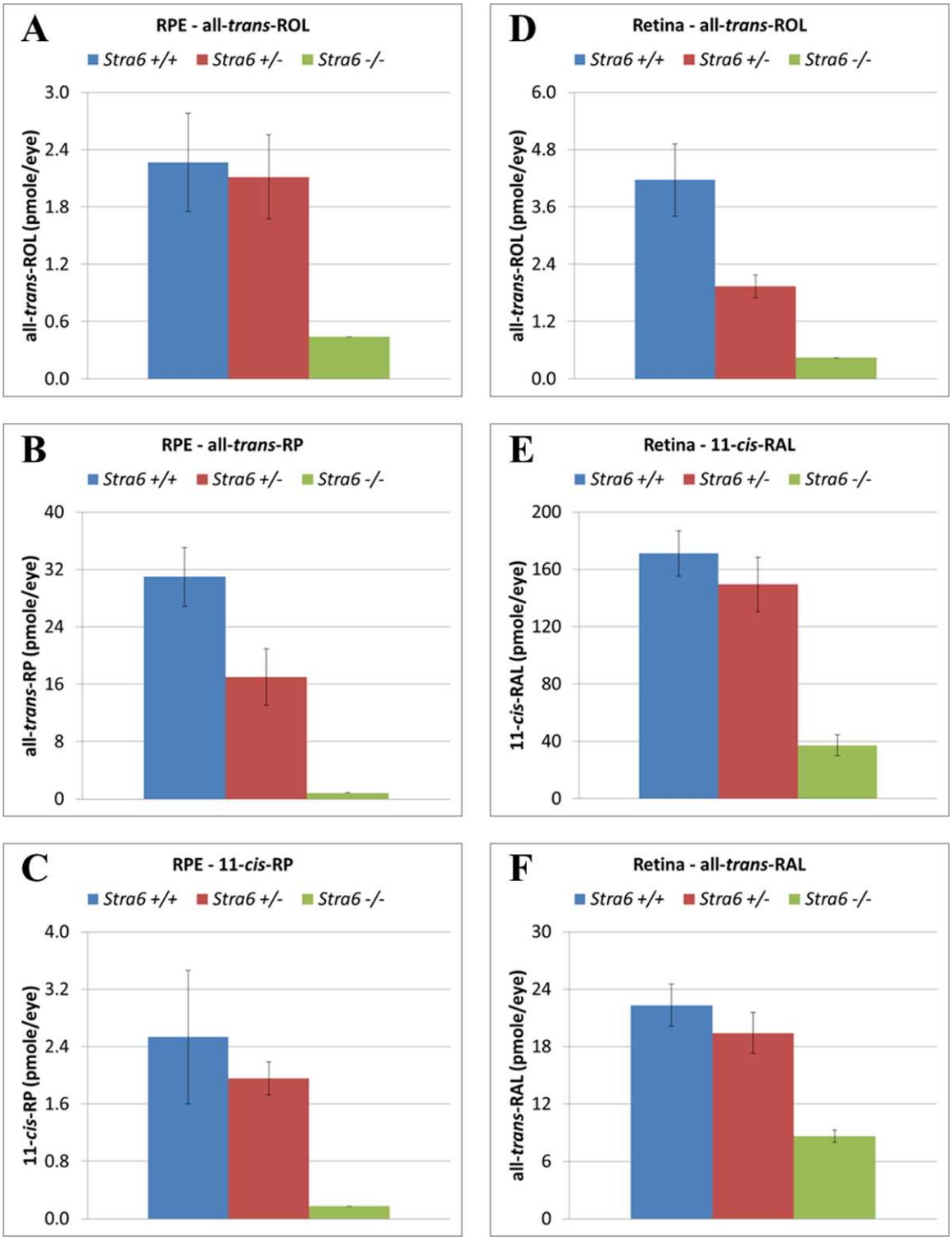

Figure 10. Retinoid content in RPE and neurosensory retina from all three *stra6* genotypes. A reduction in the levels of all-*trans*-ROL was observed in both RPE and neurosensory retina of *stra6* null mice (**A**, **D**). These mutants also showed a reduction in the content of all-*trans*-RP and 11-*cis*-RP in RPE (**B**, **C**) as well as 11-*cis*-RAL and all-*trans*-RAL in the neurosensory retina (**E**, **F**). Each value represents the average of 4 eye samples for each genotype group. All samples were collected from 6-week-old *stra6* mice. Samples were analyzed by normal-phase HPLC. all-*trans*-ROL, all-*trans*-retinol; all-*trans*-RP, all-*trans*-retinyl palmitate; all-*trans*-RAL, all-*trans*-retinal; 11-*cis*-RAL, 11-*cis*-retinal; 11-*cis*-RP, 11-*cis*-retinyl palmitate.

Acknowledgments

Scott Fish, Shannan Eddington and Kendal Kernstine provided expert technical assistance. Dr. Hui Sun assisted with critical reading of the manuscript. DB is the Dolly Green Professor of Ophthalmology at UCLA.

References

1. Niederreither K, Dollé P. Retinoic acid in development: towards an integrated view. *Nat Rev Genet*. 2008;9:541–553.
2. Dräger UC. Retinoic acid signaling in the functioning brain. *Sci STKE*. 2006:10.
3. Duester G. Retinoic acid synthesis and signaling during early organogenesis. *Cell*. 2008;134:921–931.
4. Goodman DS. Plasma retinol-binding protein. In: Sporn MB, Boberts AB, Goodman DS, eds. *The Retinoids*. New York, NY: Academic Press, Inc.; 1984:41–88.
5. Blomhoff R, Green MH, Berg T, et al. Transport and storage of vitamin A. *Science*. 1990;250:399–404.
6. Bok D, Heller J. Transport of retinol from the blood to the retina: an autoradiographic study of the pigment epithelial cell surface receptor for plasma retinol-binding protein. *Exp Eye Res*. 1976;22:395–402.
7. Heller M, Bok D. A specific receptor for retinal binding protein as detected by the binding of human and bovine binding protein to pigment epithelial cells. *Am J Ophthalmol*. 1976; 81:93–97.
8. Pfeffer BA, Clark VM, Flannery JG, Bok D. Membrane receptors for retinol binding protein in cultured human retinal pigment epithelium. *Invest Ophthalmol Vis Sci*. 1986; 27:1031–1040.
9. Kawaguchi R, Yu J, Honda J, et al. A membrane receptor for retinol binding protein mediates cellular uptake of vitamin A. *Science*. 2007;315:820–825.
10. Kawaguchi R, Yu J, Wiita P, Ter-Stepanian M, Sun H. Mapping the membrane topology and extracellular ligand binding domains of the retinol binding protein receptor. *Biochemistry*. 2008;47:5387–5395.
11. Kawaguchi R, Yu J, Wiita P, Honda J, Sun H. An essential ligand-binding domain in the membrane receptor for retinol-binding protein revealed by large-scale mutagenesis and a human polymorphism. *J Biol Chem*. 2008;30:15160–15168.
12. Kawaguchi R, Yu J, Ter-Stepanian M, et al. Receptor-mediated cellular uptake mechanism that couples to intracellular storage. *ACS Chem Biol*. 2011;6:1041–1051.
13. MacDonald PN, Bok D, Ong, DE. Localization of cellular retinol-binding protein and retinol-binding protein in cells comprising the blood-brain barrier of rat and human. *Proc Natl Acad Sci U S A*. 1990;87:4265–4269.
14. Sivaprasadarao A, Findlay JB. The interaction of retinol-binding protein with its plasma-membrane receptor. *Biochem J*. 1988; 255:561–569.
15. Sivaprasadarao A, Boudjelal M, Findlay JB. Solubilization and purification of the retinol-binding protein receptor from human placental membranes. *Biochem J*. 1994;302:245–251.
16. Pasutto F, Sticht H, Hammersen G, et al. Mutations in STRA6 cause a broad spectrum of malformations including anophthalmia, congenital heart defects, diaphragmatic hernia, alveolar capillary dysplasia, lung hypoplasia, and mental retardation. *Am J Hum Genet*. 2007;80:550–560.
17. Golzio C, Martinovic-Bouriel J, Thomas S, et al. Matthew-Wood syndrome is caused by truncating mutations in the retinol-binding protein receptor gene STRA6. *Am J Hum Genet*. 2007;80:1179–1187.
18. Chassaing N, Golzio C, Odent S, et al. Phenotypic spectrum of STRA6 mutations: from Matthew-Wood syndrome to non-lethal anophthalmia. *Hum Mutat*. 2009;30:E673–E681.
19. Isken A, Golczak M, Oberhauser V, et al. RBP4 disrupts vitamin A uptake homeostasis in a STRA6-deficient animal model for Matthew-Wood syndrome. *Cell Metab*. 2008;7:258–268.
20. Ruiz A, Bok D. Molecular characterization of lecithin retinol acyltransferase. In: Palcsewski K, ed. *Methods in Enzymology. Vol. 316*. New York, NY: Academic Press; 2000:400–413.
21. Radu RA, Hu J, Peng J, Bok D, et al. Retinal pigment epithelium-retinal G protein receptor-opsin mediates light-dependent translocation of all-trans-retinyl esters for synthesis of visual chromophore in retinal pigment epithelial cells. *J Biol Chem*. 2008;283:19730–19738.
22. Nusinowitz S, Ridder WH 3rd, Ramirez J. Temporal response properties of the primary and secondary rod-signaling pathways in normal and Gnat2 mutant mice. *Exp Eye Res*. 2007;84:1104–1114.
23. Traboulsi E. The eye. In: Stevenson RE, Halland JG, Goodman AM, eds. *Human Malformations and Related Anomalies. Vol. 2*. New York, NY: Oxford University Press, 1993;163–191.
24. Redmond TM, Yu S, Lee E, et al. Rpe65 is necessary for production of 11-cis-vitamin A in the retinal visual cycle. *Nat Genet*. 1998;20:344–351.
25. Ruiz A, Ghyselinck NB, Mata N, et al. Somatic ablation of the Lrat gene in the mouse retinal pigment epithelium drastically reduces its retinoid storage. *Invest Ophthalmol Vis Sci*. 2007; 48:5377–5387.
26. Rohrer B, Goletz P, Znoiko S, et al. Correlation of regenerable opsin with rod ERG signal in Rpe65−/− mice during development and aging. *Invest Ophthalmol Vis Sci*. 2003; 44:310–315.
27. Jin M, Li S, Nusinowitz S, et al. The role of interphotoreceptor retinoid-binding protein on the translocation of visual retinoids and function of cone photoreceptors. *J Neurosci*. 2009;29:1486–1495.
28. Warkany J, Shraffenberger S. Congenital malformations induced in rats be maternal vitamin-A deficiency. I. Defects of the eye. *Arch Ophthal*. 1946;35:150–169.
29. See AW, Clagett-Dame M. The temporal requirement for vitamin A in the developing eye: mechanism of action in optic fissure closure and new roles for the vitamin in regulating cell proliferation and adhesion in the embryonic retina. *Dev Biol*. 2009;325:94–105.
30. Ghyselinck NB, Dupé V, Dierich A, et al. Role of the retinoic acid receptor beta (RARbeta) during mouse development. *Int J Dev Biol*. 1997;41:425–447.
31. Dupé V, Matt N, Garnier JM, Chambon P, Mark M, Ghyselinck NB. A newborn lethal defect due to inactivation of retinaldehyde dehydrogenase type 3 is prevented by maternal retinoic acid treatment. *Proc Natl Acad Sci U S A*. 2003;25:14036–14041.
32. Quadro L, Blaner WS, Salchow DJ, et al. Impaired retinal function and vitamin A availability in mice lacking retinol-binding protein. *EMBO J*. 1999;18:4633–4644.
33. Quadro L, Hamberger L, Colantuoni, V, Gottesman ME, Blaner WS. Understanding the physiological role of retinol binding protein in vitamin A metabolism using transgenic and knockout mouse models. *Mol Aspects Med*. 2003;24:421–430.
34. Ghyselinck NB, Vernet N, Dennefeld C, et al. Retinoids and spermatogenesis: lessons from mutant mice lacking the plasmaretinol binding protein. *Dev Dyn*. 2006;235:1608–1622.
35. Donehower LA, Harvey M, Slagle BL, et al. Mice deficient for p53 are developmentally normal but susceptible to spontaneous tumours. *Nature*. 1992;356:215–221.

36. Sun H, Molday RS, Nathans J. Retinal stimulates ATP hydrolysis by purified and reconstituted ABCR, the photoreceptor-specific ATP-binding cassette transporter responsible for Stargardt disease. *J Biol Chem*. 1999;274:8269–8281.

37. Weng J, Mata NL, Azarian SM, et al. Insights into the function of Rim protein in photoreceptors and etiology of Stargardt's disease from the phenotype in abcr knockout mice. *Cell*. 1999; 98:13–23.

38. Ahn J, Wong JT, Molday RS. The effect of lipid environment and retinoids on the ATPase activity of ABCR, the photoreceptor ABC transporter responsible for Stargardt macular dystrophy. *J Biol Chem*. 2000;275:20399–20405.

39. Sivaprasadarao A, Findlay JB. The mechanism of uptake of retinol by plasmamembrane vesicles. *Biochem J*. 1988;255: 571–579.

40. Goodman DS, Blaner WS. Biosynthesis, absorption, and hepatic metabolism of retinol. In: Sporn MB, Roberts AB, Goodman DS, eds. *The Retinoids. Vol. 2*. New York, NY: Academic Press; 1984;2–34.

41. Christensen EI, Willnow TE. Essential role of megalin in renal proximal tubule for vitamin homeostasis. *J Am Soc Nephrol*. 1999;10:2224–2236.

42. Marinó M, Andrews D, Brown D, McCluskey RT. Transcytosis of retinol-binding protein across renal proximal tubule cells after megalin (gp 330)-mediated endocytosis. *J Am Soc Nephrol*. 2001;12:637–648.